

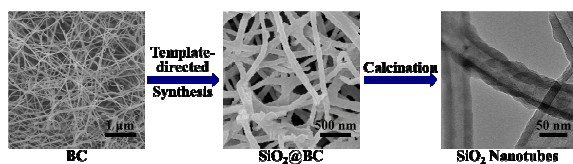


**Bacterial cellulose-templated synthesis of free-standing silica nanotubes with three-dimensional network structure**

Journal:	<i>RSC Advances</i>
Manuscript ID:	RA-COM-05-2015-008658.R1
Article Type:	Communication
Date Submitted by the Author:	21-May-2015
Complete List of Authors:	Wan, Yizao; East China Jiaotong University, Yang, Zhiwei; Tianjin University, Xiong, Guangyao; East China Jiaotong University, Raman, Sudha; Duke University, Luo, Honglin; Tianjin University,

### Table of content entry

Free-standing silica nanotubes with three-dimensional network structure were prepared via template-assisted sol-gel process by using bacterial cellulose as template and catalyst and calcination.



**Bacterial cellulose-templated synthesis of free-standing silica nanotubes with three-dimensional network structure**

Yizao Wan <sup>a,b</sup>, Zhiwei Yang <sup>b</sup>, Guangyao Xiong <sup>\*a</sup>, Sudha R Raman <sup>c</sup>, Honglin Luo <sup>\*b</sup>

<sup>a</sup> *School of Mechanical and Electrical Engineering, East China Jiaotong University, Nanchang 330013, China*

<sup>b</sup> *School of Materials Science and Engineering, Tianjin Key Laboratory of Composite and Functional Materials, Key Laboratory of Advanced Ceramics and Machining Technology, Ministry of Education, Tianjin University, Tianjin 300072, China*

<sup>c</sup> *Department of Community and Family Medicine, Duke University, North Carolina, USA*

Abstract

Nanotubes with a three-dimensional (3D) network structure are highly sought after in many fields. We report a scalable synthesis of silica nanotubes with a 3D network structure via a scalable and environmentally friendly template-assisted sol-gel route followed by calcination. The sol-gel process was conducted under ambient conditions and near-neutral pH without any additional catalysts by using bacterial cellulose (BC) as the template agent and catalyst. The formation of well-defined nanotubes and the 3D network structure were confirmed by TEM and SEM. The roles of BC nanofibers as both the catalyst and structure directing agent were demonstrated. The silica nanotubes exhibited intensive blue luminescence under UV irradiation.

Key words: Bacterial cellulose; Nanotube; Silica; Three-dimensional

The discovery of carbon nanotubes (CNTs) and their peculiar and fascinating properties have triggered extensive researches not only on CNTs but also on other inorganic nanotubes including nanotubes made of metal oxides such as SiO<sub>2</sub>, TiO<sub>2</sub>, ZrO<sub>2</sub>, Al<sub>2</sub>O<sub>3</sub>, V<sub>2</sub>O<sub>5</sub>, and MoO<sub>3</sub>.<sup>1-4</sup> Among many ceramic nanotubes, silica nanotubes have attracted tremendous attention since they are biocompatible, photoluminescent, and their surfaces are both accessible and modifiable<sup>5</sup> and thus have wide applications in, for example, gene delivery,<sup>6</sup> sensing,<sup>7</sup> and drug separation.<sup>8</sup> Among various methods available for the production of silica nanotubes, the template-directed synthesis has been most widely reported owing to its versatility, cost-effectiveness and its ability to control the physical dimensions.<sup>1</sup> However, the template syntheses usually require an external hydrolyzing agent, an organic solvent or control over the pH of the system,<sup>1</sup> which means that the synthesis conditions are not environmentally friendly.

In nature, the formation of biogenic silica is formed under ambient conditions and near-neutral pH since organic macromolecules such as silaffin peptides<sup>9</sup> and polyamines<sup>10</sup> catalyze silica formation under ambient conditions. Inspired by natural formation of silica, silica in diverse forms including nanotubes, spheres, and plates has been synthesized by this strategy utilizing various (bio)organic templates including peptide amphiphile (PA) nanofibers,<sup>1</sup> collagen fibrils,<sup>11</sup> silicatein filaments,<sup>12</sup> and polycationic peptide.<sup>9</sup> It is believed that exploring a facile and scalable preparation of templates is crucial to the large-scale production of silica nanotubes. In this context, bacterial cellulose (BC), a natural polysaccharide

synthesized by nonpathogenic microbial strains such as *Acetobacter xylinum*, shows promise since BC has long been mass produced, commercially available, and much cheaper than other organic templates mentioned above. Additionally, the high strength of BC enables it to bear the weight of deposits, the nano-sized fiber diameter makes it suitable for the deposition of nanostructured materials via replication, the high water holding capacity allows the penetration of precursors and reactants and favors reactions on the surface of each filament, and the intrinsic three-dimensional (3D) network makes it possible to acquire replicas with unique 3D network structure. Recently, BC has become an attractive template for deposition of various inorganic materials such as hydroxyapatite,<sup>13</sup> Cu<sub>2</sub>O,<sup>14</sup> TiO<sub>2</sub>,<sup>15</sup> SiO<sub>2</sub>,<sup>16</sup> and ZnO<sup>17</sup> due to its abundant hydroxyl functional groups which make the surface easily modifiable via phosphorylation and sulfation<sup>18</sup> and various oxidizations.<sup>19</sup> Although significant progress has been made in the deposition of various inorganic materials aforementioned on BC nanofibers, there has been no report on the synthesis of free-standing silica nanotubes with 3D network structures via the BC template.

For the first time, we report here a scalable two-step approach (sol-gel and calcination) for synthesizing free-standing silica nanotubes with 3D porous network structure. The sol-gel process was carried out using natural BC nanofibers as the template and catalyst without employing any additional catalyst and the calcination was conducted in air.

The preparation and cleansing procedures of BC pellicles were identical to those described in our previous work.<sup>20</sup> The detailed description is presented in the

Supporting Information. Similarly, the preparation of silica-coated BC nanofibers and silica nanotubes as well as the characterizations are also presented in the Supporting Information.

The morphologies and fiber diameter distribution of pristine BC, silica-coated BC, and silica nanotubes are shown in Fig. 1 and Fig. S1 (in the Supporting Information). Pristine BC shows typical 3D porous network structure (Fig. 1a) with an average fiber diameter of 37 nm (Fig. S1a). The 3D interconnected porous structure remains unchanged after coating with silica at the reaction temperature of 25 and -30 °C (Fig. 1b and c). The fiber diameter distribution results (Fig. S1b and c) indicate that the silica-coated BC fibers exhibit an average diameter of 93 and 69 nm at a reaction temperature of 25 and -30 °C, respectively. The fiber diameter of SiO<sub>2</sub>/BC+25 is larger than that of SiO<sub>2</sub>/BC-30 due to the faster TEOS polymerization at room temperature as compared to -30 °C. After calcination at 500 °C for 6 h, both SiO<sub>2</sub>+25 and SiO<sub>2</sub>-30 nanotubes still keep their three-dimensionality and sizes (in centimeters, comparing insets in Fig. 1b-e). Fig. S1d and e reveals that the average diameter of SiO<sub>2</sub>+25 and SiO<sub>2</sub>-30 is 63 (ranging from 34-106 nm) and 44 nm (ranging from 20-65 nm), respectively, showing a reduction as compared to SiO<sub>2</sub>/BC+25 and SiO<sub>2</sub>/BC-30 due to the evaporation of the organic species.

To further characterize these silica nanotubes, TEM was employed to acquire more detailed information on the structure. Fig. 2a and d reveals that SiO<sub>2</sub>+25 and SiO<sub>2</sub>-30 retain the 3D network structure of BC, which is consistent with SEM results. HRTEM images (Fig. 2b and e) clearly show a hollow tube structure with distinct

walls for SiO<sub>2</sub>+25 and SiO<sub>2</sub>-30. Note that, although SiO<sub>2</sub>+25 and SiO<sub>2</sub>-30 have almost the same inner diameter (around 23 nm), the outer diameter of SiO<sub>2</sub>+25 and SiO<sub>2</sub>-30 is ca. 57 and 45 nm, respectively, and their wall thickness is ca. 17 nm and 10 nm, respectively, suggesting that reaction at a higher temperature produces a thicker wall. This is understandable since temperature is one of the parameters that controls the hydrolysis and condensation reactions,<sup>21</sup> and, evidently, at a higher temperature, all reaction steps (including the hydrolysis and polycondensation of TEOS) and silica growth are faster as compared to those processes at a lower temperature.<sup>22</sup> The SAED patterns (insets in Fig. 2a and d) of both SiO<sub>2</sub>+25 and SiO<sub>2</sub>-30 indicate that the silica nanotubes obtained at both temperatures are amorphous. The EDS spectra shown in Fig. 2c and f confirm the presence of silicon and oxygen elements for both SiO<sub>2</sub>+25 and SiO<sub>2</sub>-30. TEM results clearly demonstrate that silica nanotubes with a certain wall thickness can be prepared at ambient temperature and near-neutral pH without any external catalyst and that the morphology of silica nanotubes can be adjusted by altering reaction temperature.

XRD measurement was carried out to analyze the structure of silica nanotubes. The XRD patterns of BC, silica-coated BC, and silica nanotubes and the analysis are presented in Fig. 3A. The XRD results reveal that the obtained silica nanotubes have an amorphous structure, which agrees with SAED results. The FTIR spectra of BC, SiO<sub>2</sub>/BC+25, and SiO<sub>2</sub>+25 are represented in Fig. 3B. The FTIR results confirm the presence of Si-O-C in the spectrum of SiO<sub>2</sub>/BC+25, suggesting the occurrence of a chemical reaction between hydroxyl groups on BC and silanol groups. We examined

the thermal decomposition of various samples by TGA in air atmosphere (see Fig. S2 in the Supporting Information). TGA curves show that both SiO<sub>2</sub>/+25 and SiO<sub>2</sub>/-30 are highly thermostable in air. Note that there is significant difference in the residual solid between SiO<sub>2</sub>/BC+25 and SiO<sub>2</sub>/BC-30, which reflects the effect of reaction temperature, namely a higher reaction temperature favors the formation of more SiO<sub>2</sub>.

TEOS has long been used as a silica precursor to fabricate various silica nanostructures. Generally, acid or base solution catalysts (such as H<sup>+</sup>, OH<sup>-</sup>, or benzylamine) play an indispensable role in initiating and accelerating the hydrolysis of silica precursors and the subsequent sol-gel condensation.<sup>23</sup> In template-directed synthesis, it is well documented that the functionality available on the surface of templates allows the nucleation and growth of inorganic materials at the surface,<sup>1</sup> acting as a catalyst. For instance, Yuwono and Hartgerink declared that PA nanofibers with amino and imidazole chemical functionality acted as a template and catalyst.<sup>24</sup> Previous investigations on the catalytic role of macromolecules, such as poly-(allylamine) and poly(L-lysine) hydrochloride, showed that these polymers are cationically charged in aqueous systems at near-neutral pH and catalyzed the formation of spherical silica particles from TEOS.<sup>25</sup> A study by Cha et al demonstrated that the silicatein filaments and their constituent subunits catalyzed the *in vitro* polymerization of silica at near-neutral pH.<sup>12</sup> Notably, previous studies have also reported on the formation of silica nanotubes using collagen templates.<sup>11, 26, 27</sup> Electrostatic interaction between anionic silica oligomers and the cationic collagen fibrils was believed to be responsible for the silica formation<sup>27</sup> while many

researchers thought that hydrogen bonding contributed to the silica–collagen adhesion.<sup>11,26</sup> Furthermore, the reaction of silanol with hydroxyl groups on organic polymers such as polydimethylsiloxane was reported.<sup>28</sup> The role of hydroxyl groups was also proposed by Hecky et al. who postulated that the hydroxyl-rich proteins of the silicified diatom wall might condense with silicic acid monomers, thus serving as scaffolds to organize the growth of the silica.<sup>29</sup>

The results described above indicate that silica was attracted to BC nanofibers to yield silica-coated BC fibers. However, in the present study, we added no solution catalysts to the aqueous medium, nor was BC surface modified. This infers that it is the hydroxyl groups on BC that trigger the formation of silica on the surface of BC. It is evident that the electrostatic interaction mechanism will not work between silica oligomers and the -OH groups on BC nanofibers. Therefore, hydrogen bonding is the only mechanism that is responsible for the interaction between silicate species and BC nanofibers, which is consistent with a previous report.<sup>30</sup> As a result, it can be speculated that the hydroxyl groups on BC act as not only a template but also a catalyst which catalyze the hydrolysis and condensation of silica precursors under ambient conditions and near-neutral pH. Fig. 4 schematically represents the proposed mechanism for the formation of silica nanotubes. In the first step, TEOS molecules solved in ethanol penetrate into and occupy the empty space of BC network structure. Silica oligomers are absorbed onto the surface of BC nanofibers due to the interaction between silica oligomers and hydroxyl groups on the surface of BC fibers. In the second step, when these template nanofibers are immersed in the TEOS-containing

solution of ethanol–water, hydrolysis and condensation of TEOS are carried out, and the TEOS covering the BC nanofibers will subsequently polycondensate to form a silica coating. As a result, silica-coated BC fibers are obtained. In the final step, i.e., during the calcination, these BC nanofiber templates are burned out to yield silica nanotubes. It is clear that hydroxyl groups are able to catalyze silica formation at near-neutral pH under ambient conditions. The activity of BC nanofibers which catalyze the hydrolysis and polycondensation of TEOS at near-neutral pH without external catalysts is likely due to their high surface density of hydroxyl groups originated from the fine fibers of BC.

The pore structure, volume, and pore size of silica nanotubes ( $\text{SiO}_2+25$  and  $\text{SiO}_2-30$ ) were examined by  $\text{N}_2$  adsorption–desorption experiments. The isotherm is shown in Fig. S3 and the corresponding quantitative data are summarized in Table S1 (the detailed analysis is presented in the Supporting Information). Pore structure measurements reveal that the BET surface area of  $\text{SiO}_2+25$  and  $\text{SiO}_2-30$  calculated from  $\text{N}_2$  adsorption/desorption isotherms is 177.1 and 451.0  $\text{m}^2 \text{g}^{-1}$ , respectively, and the pore volume is determined as 0.4005 and 0.8267  $\text{cm}^3 \text{g}^{-1}$ , respectively. The lower specific surface area of  $\text{SiO}_2+25$  is attributed to its denser 3D structure as revealed by TGA as compared to  $\text{SiO}_2-30$ . The significant differences in BET surface area and pore volume imply that the pore structure of silica nanotubes can be adjusted by tuning reaction temperature.

We evaluated the mechanical properties of  $\text{SiO}_2+25$  and  $\text{SiO}_2/\text{BC}+25$  by compression testing, but we failed to test  $\text{SiO}_2-30$  since it is too fragile, which, in turn,

means that the mechanical properties of SiO<sub>2</sub> nanotubes can be adjusted by reaction temperature. Fig. 5A shows the typical compression stress–strain curves of SiO<sub>2</sub>+25 and SiO<sub>2</sub>/BC+25. In general, the stress–strain curve for a foam in compression is characterized by three distinct regimes: a linear elastic regime, a collapse plateau regime and a densification regime.<sup>31</sup> The absence of the first linear elastic regime indicates that both SiO<sub>2</sub>+25 and SiO<sub>2</sub>/BC+25 are brittle in nature, which is the common weakness of ceramic scaffolds. According to previous reports,<sup>32,33</sup> we determined the compressive stresses at 40, 60, and 80% strain, as defined in literature, which are 2.5, 7.0, and 18.4 kPa, respectively, for SiO<sub>2</sub>+25, and 7.9, 20.4, and 48.7 kPa, respectively, for SiO<sub>2</sub>/BC+25. The much lower strength of SiO<sub>2</sub>+25 compared to SiO<sub>2</sub>/BC+25 is attributed to the hollow structure of SiO<sub>2</sub>+25 and its absence of the support of BC substrate. Note that the strength level of SiO<sub>2</sub>+25 is comparable to that of silica aerogel reported by Alaoui and co-workers.<sup>34</sup>

The PL emission spectra of SiO<sub>2</sub>+25 and SiO<sub>2</sub>-30 are shown in Fig. 5B. Under short wavelength UV irradiation (325 nm), both of them exhibit broad emission with a peak emission at around 440 nm (blue emission). Note that there is no significant difference in the PL intensity between SiO<sub>2</sub>+25 and SiO<sub>2</sub>-30. Under excitation with 375 nm UV light, SiO<sub>2</sub>+25 and SiO<sub>2</sub>-30 have a broader and more intensive band from 350 to 650 nm with a stronger peak at 440 nm as compared to the excitation of 325 nm light. It is clear that the PL intensity of SiO<sub>2</sub>-30 is much stronger than that of SiO<sub>2</sub>+25. Unlike conventional luminescent materials containing activators such as rare-earth and transition-metal ions, silica is a self-activated luminescent material.

Luminescence in silica has been generally attributed to defect centers in the silica, carbon/oxygen impurities, and nitrogen centered effects.<sup>35-37</sup> Zhang and co-workers believed that the bright visible photoluminescence from silica nanotubes was due to the Si-OH complex located on both the inner and outer surfaces of the nanotubes.<sup>38</sup> It seems that our PL results are consistent with the carbon/oxygen impurities mechanism and the Si-OH complex mechanism. However, the difference in PL intensity between SiO<sub>2</sub>+25 and SiO<sub>2</sub>-30 is not fully understood at this moment and more investigation is required. The PL results demonstrate that the reported silica nanotubes may be very attractive for applications in optoelectronic devices, biology labeling, and biomedicine.

In summary, a scalable two-step approach has been developed to fabricate free-standing silica nanotubes with 3D mesoporous network structure. The template-assisted sol-gel process was conducted under ambient conditions, atmospheric pressure, and near-neutral pH by using BC nanofibers as the template and catalyst without using any additional catalysts. The obtained silica nanotubes sustained the 3D porous structure of BC and showed a clear hollow tube structure with distinct walls. The strength of SiO<sub>2</sub>+25 is comparable to that of previously reported silica aerogel. The SiO<sub>2</sub>+25 exhibits strong blue emission peaking at around 440 nm under UV excitation, which makes it a potential material for application in the fields of traceable drug delivery and disease therapy.

This work is supported by the National Natural Science Foundation of China (Grant No. 51172158) and the Science & Research Foundation of Jiangxi Province

(Grant No. 20151BDH80061).

### Notes and references

1. S. Ahmed, J. H. Mondal, N. Behera and D. Das, *Langmuir*, 2013, **29**, 14274-14283.
2. G. Du, Q. Chen, R. Che, Z. Yuan and L.-M. Peng, *Appl. Phys. Lett.*, 2001, **79**, 3702.
3. P. Hoyer, *Adv. Mater.*, 1996, **8**, 857-859.
4. B. Satishkumar, A. Govindaraj, E. M. Vogl, L. Basumallick and C. Rao, *J. Mater. Res.*, 1997, **12**, 604-606.
5. T. Dennenwaldt, S. J. Sedlmaier, A. Binek, W. Schnick and C. Scheu, *J. Phys. Chem. C*, 2014, **118**, 8416-8423.
6. C. C. Chen, Y. C. Liu, C. H. Wu, C. C. Yeh, M. T. Su and Y. C. Wu, *Adv. Mater.*, 2005, **17**, 404-407.
7. S. J. Lee, S. S. Lee, J. Y. Lee and J. H. Jung, *Chem. Mater.*, 2006, **18**, 4713-4715.
8. S. B. Lee, D. T. Mitchell, L. Trofin, T. K. Nevanen, H. Söderlund and C. R. Martin, *Science*, 2002, **296**, 2198-2200.
9. N. Kröger, R. Deutzmann and M. Sumper, *Science*, 1999, **286**, 1129-1132.
10. N. Kröger, R. Deutzmann, C. Bergsdorf and M. Sumper, *Proc. Natl. Acad. Sci. U. S. A.*, 2000, **97**, 14133-14138.
11. S. Chen, A. Osaka and N. Hanagata, *J. Mater. Chem.*, 2011, **21**, 4332-4338.
12. J. N. Cha, K. Shimizu, Y. Zhou, S. C. Christiansen, B. F. Chmelka, G. D.

- Stucky and D. E. Morse, *Proc. Natl. Acad. Sci. U. S. A.*, 1999, **96**, 361-365.
13. Y. Z. Wan, Y. Huang, C. D. Yuan, S. Raman, Y. Zhu, H. J. Jiang, F. He and C. Gao, *Mater. Sci. Engin. C*, 2007, **27**, 855-864.
14. G. Liu, F. He, X. Li, S. Wang, L. Li, G. Zuo, Y. Huang and Y. Wan, *J. Mater. Chem.*, 2011, **21**, 10637-10640.
15. D. Zhang and L. Qi, *Chem. Commun.*, 2005, 2735-2737.
16. H. Sai, L. Xing, J. Xiang, L. Cui, J. Jiao, C. Zhao, Z. Li and F. Li, *J. Mater. Chem. A*, 2013, **1**, 7963-7970.
17. S. V. Costa, A. S. Gonçalves, M. A. Zaguete, T. Mazon and A. F. Nogueira, *Chem. Commun.*, 2013, **49**, 8096-8098.
18. A. Svensson, E. Nicklasson, T. Harrah, B. Panilaitis, D. L. Kaplan, M. Brittberg and P. Gatenholm, *Biomaterials*, 2005, **26**, 419-431.
19. H. Luo, G. Xiong, D. Hu, K. Ren, F. Yao, Y. Zhu, C. Gao and Y. Wan, *Mater. Chem. Phys.*, 2013, **143**, 373-379.
20. H. Si, H. Luo, G. Xiong, Z. Yang, S. R. Raman, R. Guo and Y. Wan, *Macromol. Rapid Comm.*, 2014, **35**, 1706-1711.
21. J. L. Gurav, I.-K. Jung, H.-H. Park, E. S. Kang and D. Y. Nadargi, *J. Nanomater.*, 2010, DOI: 10.1155/2010/409310.
22. Q. He, X. Cui, F. Cui, L. Guo and J. Shi, *Microporous Mesoporous Mater.*, 2009, **117**, 609-616.
23. Q. Ji, R. Iwaura, M. Kogiso, J. Jung, K. Yoshida and T. Shimizu, *Chem. Mater.*, 2004, **16**, 250-254.

24. V. M. Yuwono and J. D. Hartgerink, *Langmuir*, 2007, **23**, 5033-5038.
25. S. V. Patwardhan, C. Raab, N. Hüsing and S. J. Clarson, *Silicon Chem.*, 2003, **2**, 279-285.
26. D. Eglin, G. Mosser, M. M. Giraud-Guille, J. Livage and T. Coradin, *Soft Matter*, 2005, **1**, 129-131.
27. Y. Ono, Y. Kanekiyo, K. Inoue, J. Hojo, M. Nango and S. Shinkai, *Chem. Lett.*, 1999, 475-476.
28. H. H. Huang, B. Orlor and G. L. Wilkes, *Polym. Bull.*, 1985, **14**, 557-564.
29. R. E. Hecky, K. Mopper, P. Kilham and E. T. Degens, *Mar. Biol.*, 1973, **19**, 323-331.
30. J. Y. Shi, Q. Z. Yao, G. T. Zhou and S. Q. Fu, *Chem. Eur. J.*, 2013, **19**, 8073-8077.
31. B. A. Harley, J. H. Leung, E. C. C. M. Silva and L. J. Gibson, *Acta Biomater.*, 2007, **3**, 463-474.
32. M. Liu, C. Wu, Y. Jiao, S. Xiong and C. Zhou, *J Mater Chem B*, 2013, **1**, 2078.
33. M. Liu, L. Dai, H. Shi, S. Xiong and C. Zhou, *Materials Science and Engineering: C*, 2015.
34. A. H. Alaoui, T. Woignier, G. W. Scherer and J. Phalippou, *J. Non-Cryst. Solids*, 2008, **354**, 4556-4561.
35. Z. Hou, C. Zhang, C. Li, Z. Xu, Z. Cheng, G. Li, W. Wang, C. Peng and J. Lin, *Chem. Eur. J.*, 2010, **16**, 14513-14519.
36. A. M. Jakob and T. A. Schmedake, *Chem. Mater.*, 2006, **18**, 3173-3175.

37. T. Brankova, V. Bekiari and P. Lianos, *Chem. Mater.*, 2003, **15**, 1855-1859.
38. M. Zhang, E. Ciocan, Y. Bando, K. Wada, L. Cheng and P. Pirouz, *Appl. Phys. Lett.*, 2002, **80**, 491-493.

**Figure captions**

**Fig. 1** SEM images of pristine BC (a), SiO<sub>2</sub>/BC+25 (b), SiO<sub>2</sub>/BC-30 (c), SiO<sub>2</sub>+25 (d), and SiO<sub>2</sub>-30 (e) (insets showing photographs of various samples).

**Fig. 2** TEM (a and d, insets showing SAED patterns) and HRTEM (b and e) images and EDS spectra (c and f) of SiO<sub>2</sub>+25 (a-c) and SiO<sub>2</sub>-30 (d-f).

**Fig. 3.** XRD patterns (A) and FTIR spectra (B) of pristine BC, silica-coated BC, and silica nanotubes.

**Fig. 4** Proposed mechanism of the formation of silica nanotubes with 3D network structure templated by BC.

**Fig. 5** Compressive stress-strain curves of SiO<sub>2</sub>/BC+25 and SiO<sub>2</sub>+25 (A) and photoluminescence spectra of SiO<sub>2</sub>-30 (a and c) and SiO<sub>2</sub>+25 (b and d) nanotubes under the photon excitation of 375 (a and b) and 325 nm (c and d) at room temperature (B).

Fig. 1.

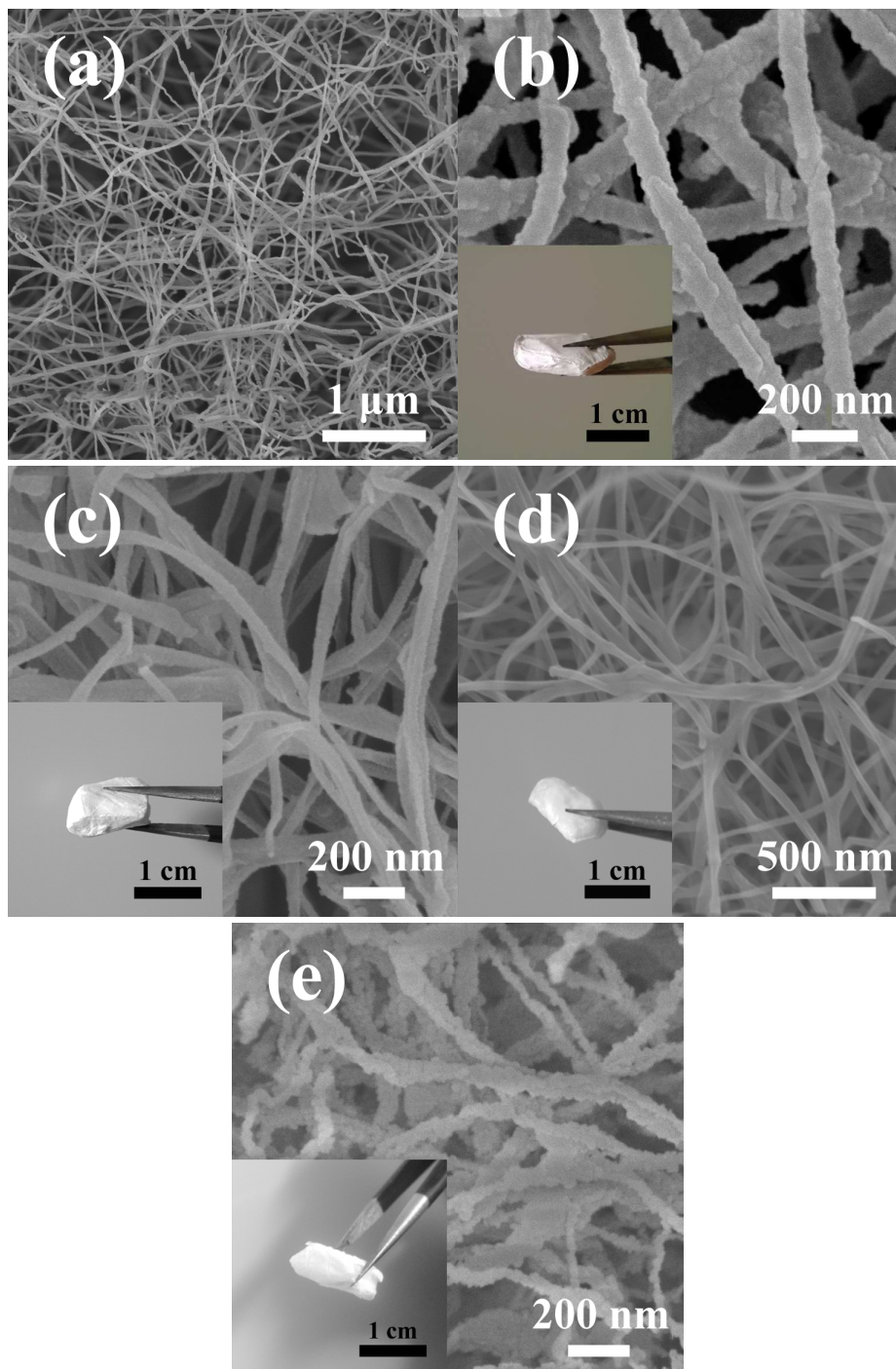


Fig. 2.

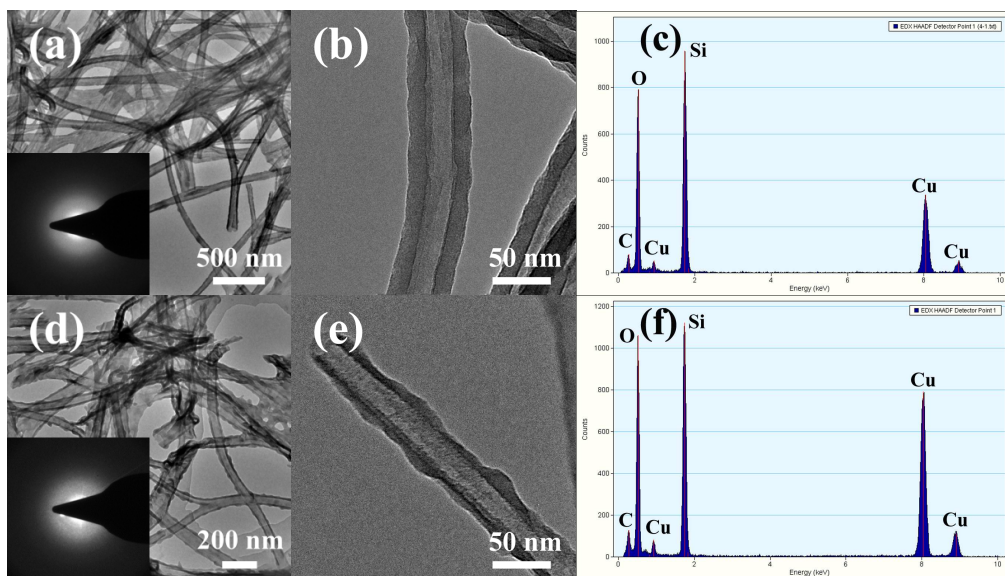


Fig. 3A.

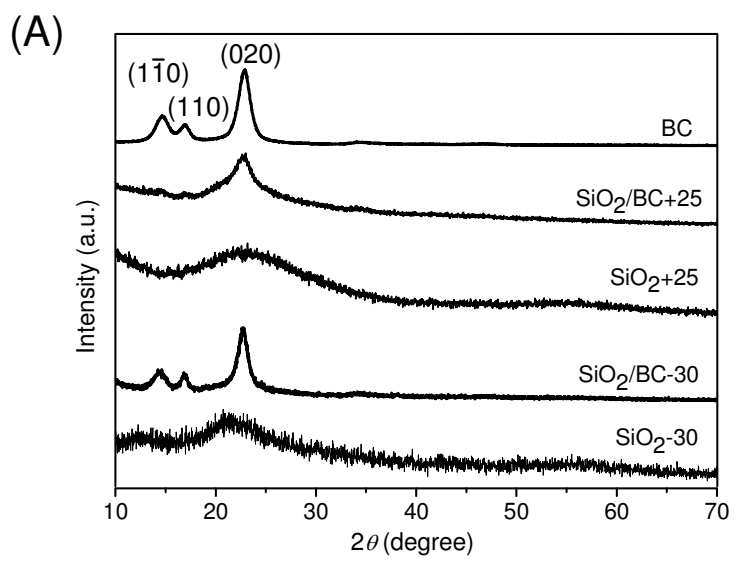


Fig. 3B.

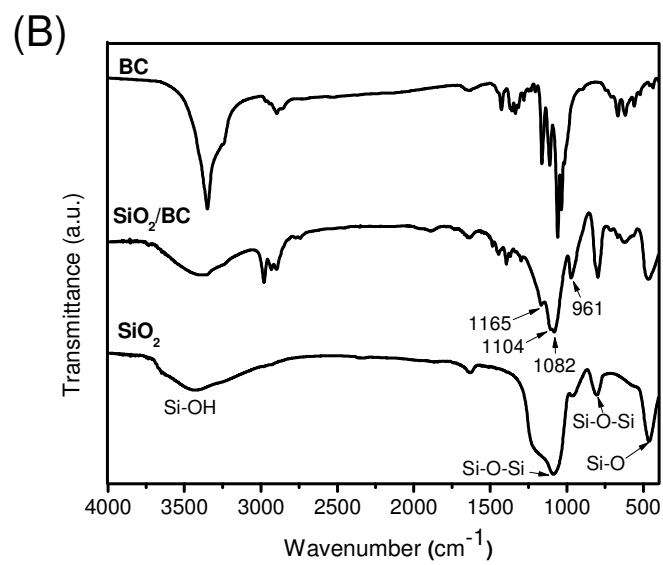


Fig. 4.

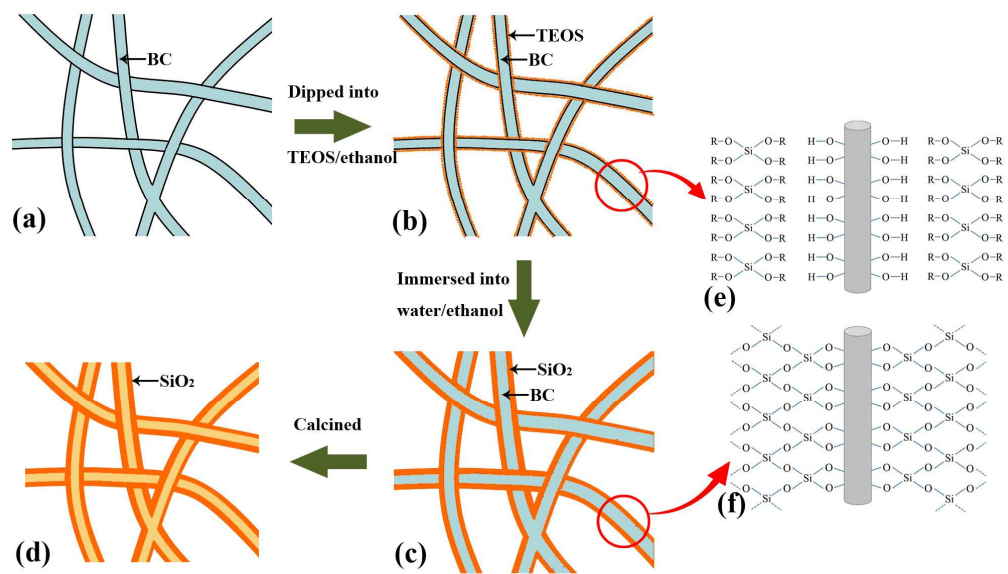


Fig. 5A.

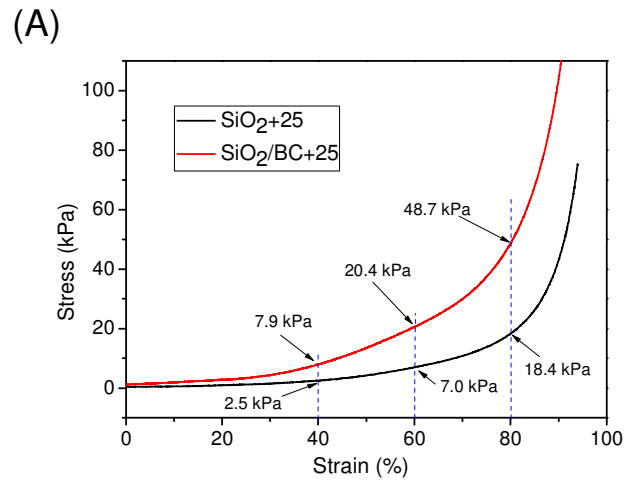


Fig. 5B.

